Coverage Dependent Adsorption of Acrolein on Pt(111) from a Combination of First Principle Theory and HREELS Study

D. Loffreda,*,† Y. Jugnet,‡ F. Delbecq,† J. C. Bertolini,‡ and P. Sautet†

Laboratoire de Chimie, UMR CNRS 5182, Ecole Normale Supérieure de Lyon, 46 Allée d'Italie, F-69364 Lyon Cedex 07, France, and Institut de Recherches sur la Catalyse, UPR CNRS 5401, 2 Avenue Albert Einstein, F-69626 Villeurbanne Cedex, France

Received: November 28, 2003; In Final Form: March 30, 2004

A combination of GGA total-energy calculations and vibrational spectra simulations with HREELS experiments is reported to obtain new insights in the stable adsorption modes of the acrolein molecule on the Pt(111) surface. The simulations of the EELS spectra have allowed us to interpret the evolution of the experimental spectra, as a function of gas exposure. A strongly bound and coverage dependent chemisorption structure is shown. The 1 L spectrum has been assigned to a low coverage η_3-cis and η_4-trans mixed phase, with the molecule lying flat on the surface and interacting by both C═C and C═O bonds. The modified spectrum for an exposure of 2 L is associated with a change in the molecule adsorption structure toward a high coverage η_2-cis and η_2-trans form on the surface in complete agreement with the DFT total energy results.

I. Introduction

Infrared reflection−absorption spectroscopy (IRRAS or RAIRS) and high-resolution electron energy loss spectroscopy (HREELS) are powerful vibrational techniques for examining clean and adsorbate-covered solid surfaces.[1−3] The vibrational spectrum of chemisorbed molecules allows in many cases the identification of the nature of the interaction between the adsorbate and the substrate by comparison with the gas-phase reference infrared spectrum. However, a thorough interpretation of the RAIRS or HREELS spectra seems to be delicate when the determination of the adsorption site is at stake. Although a wide variety of molecules have been already studied on transition metal surfaces, the interpretation of the spectra becomes a hard task for complex molecules such as $\alpha-\beta$ unsaturated aldehydes. The selective hydrogenation of these molecules is an important industrial process and much effort has been devoted to enhance the selectivity toward the unsaturated alcohol.[4−8] However, the knowledge of the interactions between such molecules and the metallic surface remains unclear even if the thermal activation of these aldehydes has been studied in order to identify the adsorption modes from the decomposition products. The adsorption of acrolein on the Pt(111) surface is a probative case where the assignment of the vibrational frequencies is not clearly cut. Actually, in a first study from RAIRS, photoemission, and near edge X-ray absorption fine structure (NEXAFS) at 95 K and ultrahigh vacuum (UHV) pressure,[9,10] the authors suggest that the molecule is physisorbed and oriented parallel to the surface. These conclusions are essentially based on the fact that only small shifts of the X-ray photoelectron spectroscopy (XPS) binding energies and of the vibration frequencies are observed. More recently, other authors have inferred from RAIRS measurements at 90 K that the acrolein molecule is initially chemisorbed with its plane parallel to the surface and interacts mainly via the carbonyl group since a red shift of the ν(C═O) stretching mode from 1724 cm^{-1} to 1681−1672 cm^{-1} is observed on the spectra.[11] No evidence of a participation of the C═C bond to the chemisorption could be obtained. Two low-temperature molecular desorption peaks were found at 115 and 145 K; however, the structure of the remaining chemisorbed acrolein on the surface above 145 K and below the molecular decomposition starting at 280 K could not be elucidated. In addition, a flat adsorption of acrolein has been proposed on Au(111)[12] and on evaporated silver films based on RAIRS and ab initio RHF/4-31G* calculations.[13,14] Acrolein initially adsorbs in a η_2(C═O) configuration, and then with the increase of temperature, a change of adsorption site is expected from η_2(C═O) to η_4(C,C,C,O) configuration. Such a transition has also been suggested from the adsorption on Rh(111).[15] However, in the case of the adsorption on TiO_2 supported Pt catalysts,[16] the observed band at 1382−1386 cm^{-1} has been assigned to the ν(C═O) stretching mode of the η_4 configuration.

Despite this important experimental effort, the attribution of the vibrational peaks to the various adsorption sites is complex and is the subject of an open debate. In our recent article,[17] the various possible adsorption structures for several $\alpha-\beta$ unsaturated aldehydes have been studied by means of density functional theory (DFT) calculations. However, this theoretical analysis has not been sufficient for a full interpretation of the previous experimental observations.

In this work, total energy calculations are presented together with the frequency calculations for the stable chemisorption sites of acrolein on Pt (111). New insights into the molecular adsorption modes are obtained by means of the comparison of the calculated EELS spectra with new experimental HREELS measurements. To do so, a method has been developed for calculating the vibrational frequencies and EELS intensities of an adsorbed molecule. Then the theoretical results are compared to the experimental HREELS observations, and an interpretation of the spectra is proposed. Compared to the infrared spectroscopy, the HREELS technique has allowed us to extend the

* To whom correspondence should be addressed. David.Loffreda@ens-lyon.fr. Fax (+33) 4 72 72 88 60.

† Laboratoire de Chimie, UMR CNRS 5182, Ecole Normale Supérieure de Lyon, 46 Allée d'Italie, F-69364 Lyon Cedex 07, France.

‡ Institut de Recherches sur la Catalyse, UPR CNRS 5401, 2 Avenue Albert Einstein, F-69626 Villeurbanne Cedex, France.

10.1021/jp037639k CCC: $27.50
Published on Web 06/02/2004

spectra to the high and low-frequency ranges by comparison with previous published RAIRS spectra.

II. Methodology

1. Experimental Methods. The whole instrumental setup is composed of two main UHV chambers separated by gate valves and with a base pressure of 4×10^{-10} Torr. The first one is equipped with various surface facilities for sputtering and annealing the sample, XPS with a dual Al/Mg X-ray source, and a quadrupole mass spectrometer (QMS). The second one is equipped with HREELS. Attached to these two UHV chambers, a small reactor equipped with a Fourier transform infrared spectrometer (NEXUS from Thermo Optek) working from UHV up to atmosphere of various gases has allowed the measurement of the infrared acrolein gas phase.

The ELS3000 (L. K. Technologies) HREELS spectrometer consists of a rotating cylindrical double pass monochromator and a double pass analyzer. Experiments were carried out with an incident beam energy of 5 eV and a resolution of 3−4 meV. All spectra were recorded in specular mode at an angle of 60° from the surface normal in the dipole scattering regime.

The Pt(111) single crystal was an aligned and polished disk (10 mm diameter, 1 mm thick), purchased from SPL (Surface Preparation Laboratory). It was cleaned by numerous Ar sputtering and annealing cycles at 1100 K until no impurity was detected by XPS.

Liquid acrolein (Sigma-Aldrich) of 95% purity was degassed by freeze−thaw cycles before introducing the gas phase through a leak valve in the HREELS chamber. Acrolein was dosed on the sample held at 180 K at various exposures defined in Langmuir ($1\ \mathrm{L} = 10^{-6}$ Torr $\times$ 1 s).

2. Calculation Techniques. The Kohn−Sham equations of the density functional theory are solved with the Vienna ab initio simulation program (VASP).[18−20] The generalized gradient approximation (GGA) of Perdew-Wang 91 has been used for the exchange-correlation functional.[21] The one-electron wave functions are developed on a basis of plane waves. The electron−ion interactions are described with Vanderbilt ultrasoft pseudopotentials[22] and a tight convergence of the plane-wave expansion was obtained with a moderate cutoff of 400 eV. Four adsorption structures and coverages have been considered: the high coverage (2×2) (1/4 ML, ML = monolayer), the medium coverage (3×2) (1/6 ML), the low coverage (3×3) (1/9 ML), and ($2\sqrt{3} \times 2\sqrt{3}$) (1/12 ML) structures. For the top site only, the high coverage ($\sqrt{3} \times \sqrt{3}$) (1/3 ML) structure has also been calculated. The surfaces are modeled by slabs containing four atomic Pt layers with an acrolein molecule adsorbed only on one side of the slab. The optimized bulk nearest neighbor separation has been chosen in all our calculations (2.82 Å). The vacuum separation between periodically repeated slabs was at least 4 bulk equivalent layers (9.2 Å). The 2D Brillouin zone integrations have been performed on $5 \times 5 \times 1$, $5 \times 5 \times 1$, $3 \times 5 \times 1$, $3 \times 3 \times 1$ and $3 \times 3 \times 1$ grids for the ($\sqrt{3} \times \sqrt{3}$), (2×2), (3×2), (3×3) and ($2\sqrt{3} \times 2\sqrt{3}$) structures, respectively. Total energy calculations with denser k-point meshes have been performed showing only small differences on the adsorption energies (<10 meV). The geometry optimizations include the acrolein molecule and the Pt atoms in the two uppermost layers of the slab, whereas the two lowest metallic planes were frozen in a bulklike geometry.

The technique for calculating the acrolein molecular frequencies is based on the numerical calculation of the second derivatives of the potential energy surface within the harmonic approach. The vibrational treatment is greatly simplified by neglecting the coupling between the molecular vibrations and the surface metallic phonons. This approximation is valid as long as the molecular frequencies are sufficiently hard (>400 cm^{-1}) so that the coupling with the metallic phonons lying in the 0−200 cm^{-1} range is weak. The force constant matrix or Hessian dynamical matrix is built with finite differences of the first derivatives of the total energy by geometrical perturbations of the optimized Cartesian coordinates of the system (±0.005 Å at the harmonic level). The diagonalization of this matrix provides the harmonic molecular frequencies and the associated harmonic normal vibration modes Q_k obtained with a matrix of weights (P_{ij}).

The first derivatives of the dynamic dipole moment are then calculated to estimate the EELS intensities for each normal mode of the stable adsorption states. In the specular mode, the main contribution to the intensity is the z-component of the dynamic dipole moment and the numerical calculation of its first derivative $\mathrm{d}\mu_z/\mathrm{d}Q_k$ with respect to a given normal mode Q_k is performed in the Cartesian coordinate system Δr_i by finite differences ($\partial\mu_z/\partial\Delta r_i$). From the dipole scattering mechanism, the absolute intensities I_{loss} of the energy losses normalized to the elastic peak intensity I_{elastic} are expressed as[2]

$$\frac{I^k_{\mathrm{loss}}}{I_{\mathrm{elastic}}} \propto \theta_{\mathrm{ads}} \frac{F(\omega_k)}{\omega_k}\left(\frac{\mathrm{d}\mu_z}{\mathrm{d}Q_k}\right)^2 = \theta_{\mathrm{ads}} \frac{F(\omega_k)}{\omega_k}\left(\sum_{i=1}^{3N} \frac{1}{\sqrt{m_i}} \frac{\partial\mu_z}{\partial\Delta r_i} P_{ki}\right)^2 \quad (1)$$

$$F(\omega_k) = \sqrt{(1-2\theta_{\mathrm{E}})}\left(\frac{\hat{\theta}_{\mathrm{c}}^{\,2}}{1+\hat{\theta}_{\mathrm{c}}^{\,2}}(\sin^2(\theta_{\mathrm{I}}) - 2\cos^2(\theta_{\mathrm{I}})) + (1+\cos^2(\theta_{\mathrm{I}}))\ln(1+\hat{\theta}_{\mathrm{c}}^{\,2})\right) \quad (2)$$

$$\theta_{\mathrm{E}} = \frac{h\omega_k}{2E_I};\ \hat{\theta}_{\mathrm{c}} = \frac{\theta_{\mathrm{c}}}{\theta_{\mathrm{E}}} \quad (3)$$

where E_{I} is the primary energy of the electron beam (5 eV), θ_{I} is the incident angle of the electron beam (60°) defined relative to the normal of the sample, and θ_{c} is the acceptance angle of the spectrometer (3°).

The numerical accuracy has been considered carefully for all of our calculations and simulations (vibrations and intensities). There are two main sources of error. An error that could be called "numeric" is due to the finite numerical accuracy of the calculations. Regarding the frequency and the intensity calculations, the numerical error has been estimated by changing the sampling and the geometrical perturbation in the finite differences technique during the derivative computations of the forces and the dipole moment. The expected numeric error for the frequency calculation technique is of the order of 10 cm^{-1} and the one for the EELS intensity is negligible. A second error which could be called "systematic" is due to the use of density functional theory (DFT). The estimate of this error is much more difficult and requires the comparison between theory and experiments in several different cases.

III. DFT Calculations and HREELS Measurements

1. Energetics and Geometry. The gas-phase acrolein has been optimized in a periodic box of $13 \times 13 \times 20$ $\mathrm{Å}^3$. Since acrolein exhibits a conformational rotational isomerism between s-trans and s-cis forms, both rotamers have been considered. The s-trans conformer or *trans*-acrolein has been found more stable by 2.3 kcal mol^{-1} (0.1 eV), which corresponds roughly

TABLE 1: DFT Optimized Geometrical Parameters of the Gas Phase Acrolein for Both s-cis and s-trans Rotamers[a]

	trans-acrolein						*cis*-acrolein		
	this work	exp[b]	error (%)	RHF 4-21G[c]	RHF 4-31G[d]	RHF 6-31G*[e]	this work	exp[b]	error (%)
$d(C_1H_1)$	1.118	1.113	0.4	1.089	1.085	1.095	1.114	1.106	0.7
$d(C_2H_2)$	1.090	1.084	0.5	1.072	1.072	1.076	1.091	1.088	0.3
$d(C_3H_3)$	1.091	1.090	0.1	1.075	1.074	1.077	1.087	1.081	0.6
$d(C_3H_4)$	1.087	1.080	0.6	1.072	1.071	1.075	1.090	1.098	−0.7
$d(C_1{=}O)$	1.225	1.214	0.9	1.212	1.212	1.190	1.226	1.215	0.9
$d(C_1{-}C_2)$	1.466	1.468	−0.1	1.477	1.463	1.478	1.479	1.478	0
$d(C_2{=}C_3)$	1.338	1.340	−0.1	1.316	1.320	1.321	1.338	1.340	−0.1
$\alpha(C{-}C{=}O)$	124.7	124.0	0.6	124.0	123.3	124	124.7	124.2	0.4
$\alpha(C{=}C{-}C)$	120.6	120.4	0.2	121.0	122.5	121	122.0	121.5	0.4
$\alpha(O{=}C{-}H_1)$	120.9	121.3	−0.3	121.2	120.2	121	120.1	120.1	0
$\alpha(C{=}C{-}H_2)$	122.4	122.4	0	122.5	122.1	122	121.5	121.1	0.3
$\alpha(C{=}C{-}H_3)$	120.6	119.7	0.7	121.6	121.7	121	122.1	121.5	0.5
$\alpha(C{=}C{-}H_4)$	122.4	122.2	0.2	122.3	122.0	122	120.0	118.5	1.3
$\alpha(CH_3H_4)$	117.0	118.1	−0.9	116.1	116.3	117	117.9	120.0	−1.7

[a] The distances are expressed in Å, and the bond angles are in degrees (°). The relative errors (%) between theoretical and experimental values[24] are also reported. Other optimized values within the restricted Hartree−Fock scheme (RHF) are indicated. [b] Reference 24. [c] Reference 27. [d] Reference 28. [e] Reference 29.

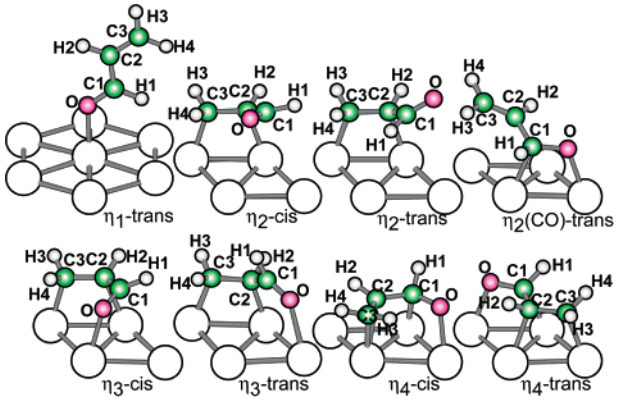

Figure 1. Lateral views of the adsorption sites. The large white balls are the surface Pt atoms, and the other atom types and numbers are explicitly defined.

to 98% of s-trans and 2% of s-cis, to be compared with 1.6 ± 0.2 kcal mol^{-1} and 96% (trans) and 4% (cis) determined experimentally at room temperature.[23] The optimized geometries are reported in Table 1. The values obtained are in an excellent agreement with the experimental ones.[24−26] The agreement is even better for the C−H distances by comparison with the previously calculated values at the RHF/4-21G,[27] 4-31G,[28] and 6-31G*[29] levels. Therefore, the VASP program, which is usually used for the calculations of periodic systems, gives also reliable results for isolated molecules.

The stable adsorption forms are reported in Figure 1 and the optimized geometries in Table 2. The corresponding adsorption energies, expressed per surface unit area, are plotted in Figure 2 as a function of acrolein surface coverage. The results presented here are complementary to those published previously.[17]

The η_1 adsorption mode (trans conformer shown in Figure 1) where the molecule is bonded to the surface only by the O atom is the less stable one. In this case, the Pt−O bond is significantly strong (d_{Pt-O} = 2.24 Å) and the C=O bond length is slightly longer than in the gas phase (1.25 Å). For all of the considered coverages, the top-trans site is never competitive.

Three stable adsorption positions are possible for the η_2 adsorption family (di-σ(C=C) and di-σ(C=O) forms; cf. Figure 1). Both cis and trans conformers are stabilized by an interaction between their C=C bond and two surface Pt atoms giving the η_2-cis and η_2-trans structures, respectively. In these cases, the C=C bond is elongated (1.48 Å) by comparison with the gas phase (1.338 Å). The Pt−C bonds are similar for both sites (2.12−2.16 Å). The O atom does not interact with the surface. These η_2(C=C) forms have almost the same adsorption energies. For the low coverage range (below 0.15 ML cf. area (I) in Figure 2), these adsorption modes are not competitive. The η_2-cis form

TABLE 2: DFT Optimized Geometries for the Various Adsorption Sites at the Coverage 1/9 ML[a]

	η_1-trans	η_2-cis	η_2-trans	η_3-cis	η_3-trans	η_4-cis	η_4-trans
$d(C_1H_1)$	1.11	1.10	1.12	1.10	1.11	1.10	1.11
$d(C_2H_2)$	1.09	1.10	1.09	1.09	1.10	1.09	1.10
$d(C_3H_3)$	1.09	1.09	1.09	1.09	1.09	1.09	1.09
$d(C_3H_4)$	1.09	1.09	1.10	1.09	1.10	1.09	1.10
$d(C_1{=}O)$	1.25	1.23	1.22	1.27	1.24	1.33	1.32
$d(C_1{-}C_2)$	1.45	1.49	1.49	1.45	1.49	1.47	1.49
$d(C_2{=}C_3)$	1.34	1.48	1.48	1.48	1.51	1.41	1.48
$d(Pt{-}C_1)$						2.23	2.24
$d(Pt{-}C_2)$		2.16	2.16	2.20	2.10	2.32	2.17
$d(Pt{-}C_3)$		2.12	2.12	2.10	2.12	2.17	2.12
$d(Pt{-}O)$	2.24			2.25	2.40	2.13	2.13
$\alpha(C{-}C{=}O)$	121.6	124.3	124.6	123.7	128.7	118.9	119.6
$\alpha(C{=}C{-}C)$	120.7	117.3	115.6	117.6	115.7	123.2	116.2
$\alpha(O{=}C{-}H_1)$	120.0	120.7	121.3	117.9	116.8	115.2	114.7
$\alpha(C{=}C{-}H_2)$	122.3	115.5	115.5	117.3	112.1	119.5	117.5
$\alpha(C{=}C{-}H_3)$	122.0	114.2	114.1	113.4	114.1	118.7	114.8
$\alpha(C{=}C{-}H_4)$	120.8	113.1	114.3	113.4	114.5	118.6	114.9
$\alpha(CH_3H_4)$	117.2	113.3	112.1	112.7	112.1	116.3	112.4

[a] The distances are expressed in Å, and the bond angles are in degrees (°).

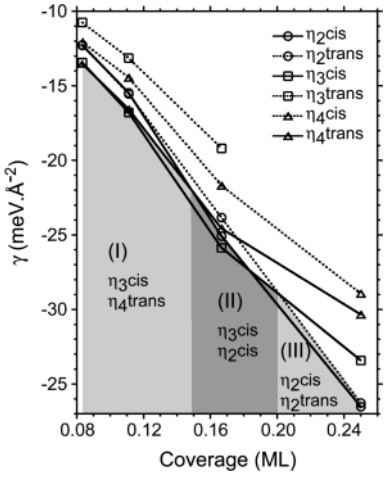

Figure 2. Adsorption energy per surface unit area γ (meV.Å^{-2}) diagram for the η_2, η_3, and η_4 site families as a function of the acrolein coverage (ML).

TABLE 3: DFT Harmonic Molecular Frequencies Compared to Experimental Infrared (300 K, 1 Torr) and HREELS (180 K, 10 L) Vibrational Bands (cm^{-1}) for the Gas Phase *trans*- and *cis*-Acrolein[a]

	trans-acrolein					*cis*-acrolein		
cm^{-1}	$\omega_{calc.}$	$\omega_{exp.}$[b]	error (%)	IR this work	HREELS 10 L this work	$\omega_{calc.}$	$\omega_{exp.}$[c]	error (%)
$\nu(C_1H_1)$	2805	2800	0.2	2800	2820	2836		
$\nu(C_2H_2)$	3027	2998	1.0	nr	3020	3003		
$\nu^{oop}(CH_3H_4)$	3143	3103	1.3	3104	3080	3177		
$\nu^{ip}(CH_3H_4)$	3054	3069	−0.5	2999	2980	3083		
$\nu(C_1{=}O)$	1691	1724	−1.9	1722	1672	1702	1722	−1.2
$\nu(C_2{=}C_3)$	1614	1625	−0.7	1627	1610	1599	1624	−1.5
$\nu(C_1{-}C_2)$	1129	1158	−2.5	1157	1153	906	919	−1.4
$\delta(C_1H_1)$	1343	1360	−1.2	1357	1360	1375		
$\delta(C_2H_2)$	1254	1275	−1.6	1272	1275	1273	1285	−0.9
$\delta(CH_3H_4)$	1403	1420	−1.2	1420	1410	1392	1403	−0.8
$\rho(CH_3H_4)$	873	912	−4.3	911	910	1028		
$\delta(C{-}C{=}O)$	565	564	0.2		nr	648		
$\delta(C{=}C{-}C)$	313	324	−3.4		325	282	276	2.2
$\gamma^{ip}(CH)$	991	993	−0.2	994	980	994	988	0.6
$\gamma^{oop}(CH)$	971	972	−0.1	nr	980	1001	1005	−0.4
$\omega(CH_3H_4)$	964	959	0.5		980	980	970	1.0
$\tau(CH_3H_4)$	591	593	−0.3		605	538	544	−1.1
$\tau(C_1{-}C_2)$	168	158	6.3			141	138	2.2

[a] The relative error (%) between theoretical and experimental values is reported. The normal modes are organized in three different families (see also Figure 5): the stretching vibrations including the in-phase $\nu^{ip}(CH_3H_4)$ and out-of-phase $\nu^{oop}(CH_3H_4)$ modes, the in-plane bending vibrations including the scissor $\delta(CH_3H_4)$ and rocking $\rho(CH_3H_4)$ modes, and the out-of-plane torsion vibrations including the in-phase $\gamma^{ip}(CH)$ and out-of-phase $\gamma^{oop}(CH)$, the wagging $\omega(CH_3H_4)$ and twisting $\tau(CH_3H_4)$ vibrations. "nr" stands for not resolved. [b] Reference 28. [c] References 33 and 34.

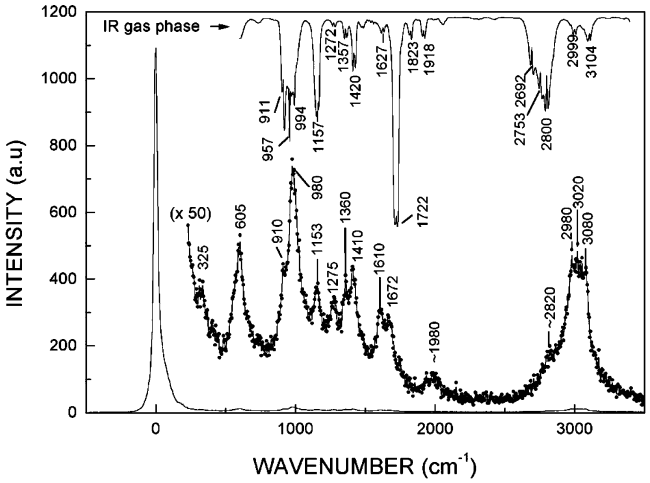

Figure 3. HREELS spectrum for 10 L acrolein adsorbed on Pt (111) at 180 K. Dots correspond to experimental data; continuous lines are drawn for a purpose of clarity. These spectra have been measured in specular mode. The infrared spectrum of gaseous acrolein (1 Torr at 300 K) is reported for comparison.

becomes competitive above 0.15 ML (cf. area (II) in Figure 2). For the high coverage regime (between 0.20 and 0.25 ML cf. area (III) in Figure 2) both η_2-cis and η_2-trans are the most stable forms. Another stable structure is the di-σ(C═O) position for the trans conformer where the C═O bond interacts with two surface Pt atoms. Since this is one of the least stable configurations, the results have not been reported here.

For the η_3 adsorption family, the acrolein C═C bond interacts with the surface as for a di-σ(C═C) form but moreover the O atom interacts also with a surface Pt atom. Both cis and trans conformers are stable leading to the respective η_3-cis and η_3-trans cases (cf. Figure 1). Due to the Pt−O interaction (with Pt−O distances of 2.25 Å for η_3-cis), the C═O bond is weakened and the C−O distance is lengthened (1.27 Å for η_3-cis) with respect to the gas-phase reference. For a wide range of coverage (between 0.08 and 0.20 ML cf. areas (I) and (II) in Figure 2), the η_3-cis form is one of the most stable sites. In contrast, the η_3-trans position is not stable anymore for the high coverage structure (1/4 ML) where the Pt−O bond is broken, giving finally the η_2-trans mode during the optimization process.

When both acrolein C═C and C═O bonds interact with the surface Pt atoms, the resulting flat adsorption forms belong to the so-called η_4 site family. In the case of the cis conformer, the η_4-cis is associated with a π interaction for C═C (2.17−2.32 Å) and di−σ for C═O (2.13−2.23 Å) (cf. Figure 1). This leads to a strong elongation of the C═O bond (1.33 Å) and a slight shortening of the C═C bond (1.41 Å) with respect to the η_2 and η_3 cases. For the trans conformer, the C═C and C═O bonds interact with the surface Pt atoms through di-σ(C═C) (d_{Pt-C} = 2.12−2.17 Å) and di-σ(C═O) forms (d_{Pt-O} = 2.13 and d_{Pt-C} = 2.24 Å). As seen for η_4-cis, the C═O bond is strongly elongated (1.32 Å). Moreover, the C═C distance is even longer (1.48 Å). The surface free adsorption energy results show that the η_4-cis form is never competitive whatever the coverage (cf. Figure 2). In contrast, η_4-trans is as competitive as the η_3-cis form for coverages below 0.15 ML (cf. area (I) in Figure 2). For higher coverages, this structure becomes less stable.

2. Vibrational Analysis. *a. HREELS Results.* The HREELS spectrum obtained for a high exposure (10 L) of acrolein on Pt(111) dosed at 180 K is shown in Figure 3 and compared to the gas phase spectrum measured by infrared spectroscopy under 1 Torr at 300 K. For such high exposures, the spectrum is dominated by molecules which are weakly interacting with the surface. The presence of more strongly bonded molecules could not be excluded as it will be discussed below. It could not correspond to a multilayer since, according to Zaera et al.,[7] the dosing temperature (180 K) is too high. However, the comparison of this spectrum with gas phase IR results is addressed and allows the identification of HREELS bands for the weakly interacting molecules.

Compared to the gas phase, most of the measured bands in the chemisorbed phase of the 10 L spectra are only slightly shifted (cf. Table 3), by less than 10 cm^{-1} toward lower wavenumber, indicating a small perturbation of the molecule. Larger shifts are observed for the $\nu(C_1H_1)$ (+20 cm^{-1}), $\nu^{ip}(CH_3H_4)$ (−19 cm^{-1}), $\nu^{oop}(CH_3H_4)$ (−24 cm^{-1}), and ν(C═O) stretching vibration (−50 cm^{-1}). Due to the orientation of

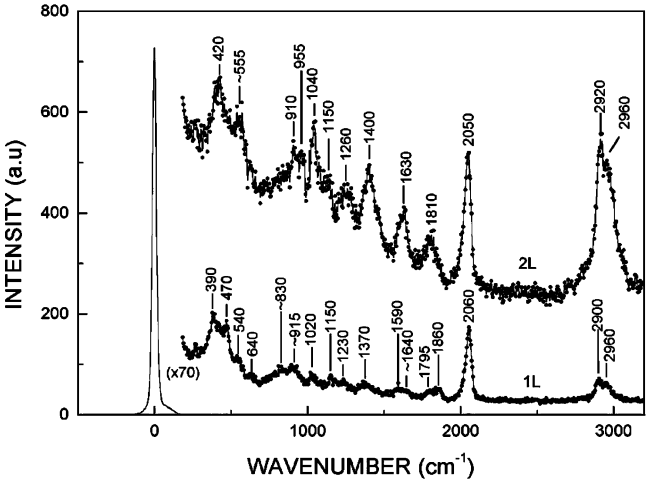

Figure 4. HREELS spectra of 1 and 2 L acrolein adsorbed on Pt(111) at 180 K. The clean surface was exposed to a pressure of 10^{-8} Torr for 100 seconds (1 L), and for 200 s (2 L). Dots correspond to experimental data; continuous lines are drawn for a purpose of clarity. Each spectrum has been normalized to the elastic peak.

the molecule by the surface, the relative band intensities are not conserved when going from the gas phase to the weakly interacting phase. Moreover, the observed bands at 1610 and 1672 cm^{-1}, which could not be characteristic of a weakly adsorbed molecular phase, suggests the presence of more tightly bonded species as it will be discussed later on. These results are in close agreement with previous infrared results,[9,11] but the reported HREELS spectrum displays more vibrational bands since it was performed in a larger wavenumber range.

In Figure 4, HREELS spectra measured at 180 K are compared for exposures of 1 and 2 L. A first remark concerns the width of the bands. A mixture of various adsorption states could be at the origin of the wide bands observed in the whole spectrum. In addition to the acrolein vibrational bands which will be discussed below, extra bands measured at 2040−2060 and 1795−1810 cm^{-1} are assigned to residual CO which chemisorbs during the spectrum acquisition. A band due to the Pt−CO stretching mode is also expected around 470 cm^{-1}. By comparison to the 10 L spectrum previously described, drastic changes are observed.

The characteristic vibrations of acrolein at 3080, 980, and 605 cm^{-1} have completely disappeared. The ν(CH) stretching bands are shifted toward lower wavenumbers indicating an interaction of the C atoms with the surface. The observation of new bands below 650 cm^{-1} indicates that strong interaction with platinum has occurred. For 1 L, all of the bands have a very weak intensity. This is in favor of an orientation of the molecule parallel to the surface since in specular mode dipole scattering is predominant, and only dipoles which have a component along the normal to the surface will be detected on a metallic surface. When increasing the exposure, the vibrational bands at 1630, 1400, and 1040 cm^{-1} become more intense. A complete interpretation of these data will be given below on the basis of the theoretical results.

b. Theoretical Approach. The calculations of the molecular vibrations in the gas phase are reported in Table 3 for both s-trans and s-cis rotamers. A good agreement (∼1→4% of error except for the low-frequency vibration $\tau(C_1-C_2)$) with previous experimental values is obtained for the harmonic frequencies. The general compatibility between theoretical results and experiments shows that the calculated harmonic frequencies are reliable for interpreting the measured spectra and so anharmonic contributions can be neglected in a first approximation. Previous semiempirical CNDO/2[30] and AM1[31] results have been published showing a good agreement with our DFT calculations.

All of the vibration modes have been organized in three different families for both conformers (cf. Table 3 and Figure 5): seven stretching modes have been reported including the C═C and C═O stretching vibrations, six in-plane bending vibration modes, and five out-of-plane torsion modes. The C_1-H_1 stretching mode, which is the softest C−H mode, is characteristic of the acrolein molecule. The only vibration that could help to recognize the s-cis and s-trans conformers is $\nu(C_1-C_2)$ which is harder for the trans conformer (1129 cm^{-1}) than for the s-cis molecule (906 cm^{-1}). For the bending modes, the characteristic vibration is the rocking mode $\rho(CH_3H_4)$ which is soft in the case of the trans conformer (873 cm^{-1}) and hard for the cis conformer (1028 cm^{-1}). For the torsion mode family,

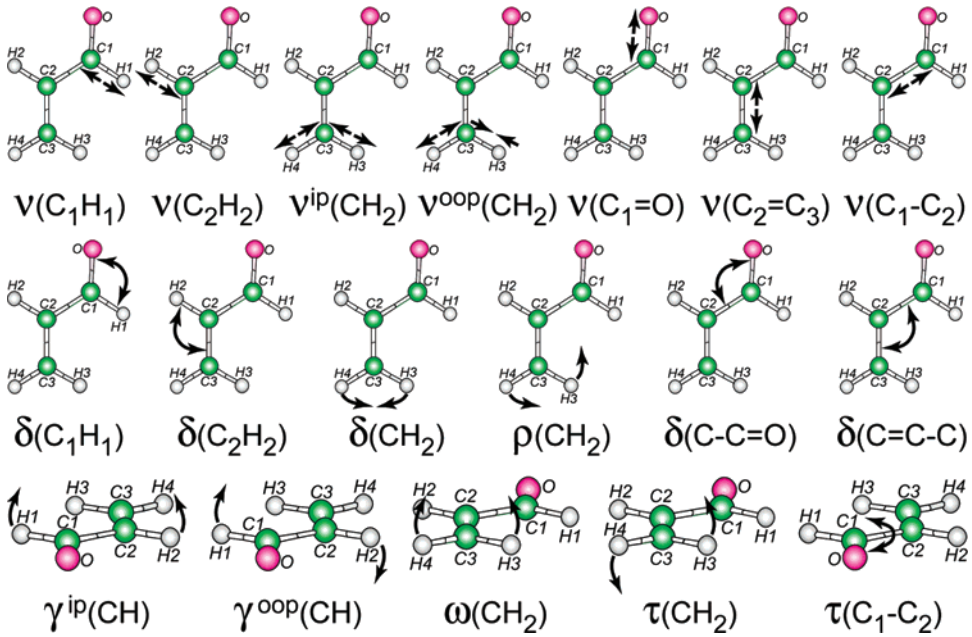

Figure 5. Schematic views of the molecular vibration normal modes for the gas phase trans-acrolein. The black arrows show the way the atoms vibrate for each mode.

TABLE 4: DFT Harmonic Molecular Frequencies (cm^{-1}) for the Various Adsorption Sites at the Low Coverage 1/9 ML and at the High Coverage 1/4 ML Only for η_2-cis and η_2-trans Sites[a]

	η_1-trans	η_2-cis		η_2-trans		η_3-cis	η_3-trans	η_4-cis	η_4-trans
coverage	1/9	1/9	1/4	1/9	1/4	1/9	1/9	1/9	1/9
$\nu(C_1H_1)$	2906	2859	2906	2716	2717	2956	2867	2958	2911
$\nu(C_2H_2)$	3118	3020	2985	3045	3045	3067	2934	3083	2999
$\nu^{oop}(CH_3H_4)$	3177	3091	3074	3082	3109	3088	3077	3158	3086
$\nu^{ip}(CH_3H_4)$	3083	3011	3014	2999	3004	3008	2998	3070	2994
$\nu(C{=}O)$	1563	1645	1632	1677	1665	1445	1584	1165	1192
$\nu(C_2{=}C_3)$	1607	1106	1118	1063	1073	1111	1035	1444	1098
$\nu(C_1{-}C_2)$	1157	856	877	931	949	918	936	888	1009
$\delta(C_1H_1)$	1324	1353	1360	1339	1360	1303	1327	1305	1312
$\delta(C_2H_2)$	1269	1303	1306	1256	1264	1342	1230	1205	1230
$\delta(CH_3H_4)$	1412	1389	1398	1400	1393	1390	1397	1360	1408
$\rho(CH_3H_4)$	930	1046	1042	1117	1125	1059	1081	1023	914
$\delta(C{-}C{=}O)$	606*	637	658	583	589	633	586	648	558
$\delta(C{=}C{-}C)$	406	313	361	350	369	354*	335	310	355
$\gamma^{oop}(CH)$	977	964	967	953	937	894	908	931	849
$\gamma^{ip}(CH)$	1001	873	872	912	900	833	769	798	746
$\omega(CH_3H_4)$	958	1030	1065	1019	1033	1025	1022	961	1039
$\tau(CH_3H_4)$	595	761	772	708	706	771	705	758	707
$\tau(C_1{-}C_2)$	309	232	259	213	239	237*	208*	526*	459*
$\nu_1(Pt{-}\eta)$	151*	^{oop}536	^{oop}527	^{oop}508	^{oop}505	^{oop}520	^{oop}530	^{oop}526*	^{oop}513*
$\nu_2(Pt{-}\eta)$		^{ip}411	^{ip}404	^{ip}395	^{ip}401	^{ip}381	^{oop}423	^{oop}410*	^{oop}459*
$\nu_3(Pt{-}\eta)$						130*	^{ip}265*	^{oop}358*	^{oop}403*
$\nu_4(Pt{-}\eta)$								^{ip}302*	^{ip}299*

[a] The normal mode notations are given in Table 3. For the metal−adsorbate stretch family $\nu(Pt{-}\eta)$, the in-phase (ip) and out-of-phase (oop) modes are indicated on the top of the left-hand side of the frequency value. The vibrations coupled with the Pt−O stretch are shown with an asterisk.

unfortunately, there is no characteristic vibration distinguishing the two rotamers.

The calculated harmonic molecular frequencies for the various adsorption forms are reported in Table 4, at the low coverage 1/9 ML for all of the adsorption modes but also at the high coverage 1/4 ML for both stable η_2-cis and η_2-trans forms. The notations chosen in Figure 5 for the gas-phase references are kept to define the modes of adsorbed states even if these modes are coupled in this latter case. The same modes as in the gas phase are found together with additional $\nu(Pt{-}\eta)$ substrate-molecule normal vibration modes. The number of these latter stretching modes depends on the coordination number of the adsorbed molecule (i.e., the number of Pt atoms involved in the adsorption). The in-phase (ip) $\nu(Pt{-}\eta)$ stretching modes are always the softest ones of this family. These soft vibrations are approximate since the coupling with the Pt surface phonons has been neglected in the generation of the force constant matrixes. For the η_2, η_3, and η_4 adsorption modes, between one and three respective out-of-phase (oop) $\nu(Pt{-}\eta)$ vibrations have also been found. Unfortunately, these modes are not characteristic of a specific site since all of the stretching frequencies lie in a narrow frequency range.

The other stretching modes are the internal molecular vibrations already mentioned for gas-phase acrolein. For the $\nu(C{-}H)$ vibrations at the low coverage 1/9 ML, the coupled in-phase $\nu^{ip}(CH_3H_4)$ and out-of-phase $\nu^{oop}(CH_3H_4)$ modes are globally shifted to the lower frequencies by comparison with the gas phase (excepted for the η_1-trans site). No clear trend emerges for $\nu(C_2H_2)$. Since the $\nu(C_1H_1)$ mode is softer for η_2-cis and η_2-trans (2859 and 2716 cm^{-1} respectively) and harder for η_3-cis and η_4-trans (2956 and 2911 cm^{-1} respectively), it could be characteristic of the presence of an η_2 structure. The $\nu(C{=}O)$ vibration is strongly softened for the adsorption sites presenting a Pt−O bond (η_1-trans, η_3-cis, and η_4-trans with respective frequencies 1563, 1445, and 1192 cm^{-1}), whereas it is slightly softened for the η_2-cis and η_2-trans sites (1645 and 1677 cm^{-1}, respectively). Therefore, a band in the 1620−1700 cm^{-1} region could be distinctive of an η_2 adsorption. The Pt−C interactions result in a strong shift of the $\nu(C{=}C)$ mode toward the low frequencies (from 1599−1614 to 1035−1111 cm^{-1}), so this vibration cannot be an indicator of a specific site. The $\nu(C{-}C)$ frequency, which is less affected by the adsorption process, can be a characteristic mode of η_2 adsorption. In the case of η_2-cis, it is shifted to the lower frequencies (856 cm^{-1}) with respect to the gas phase (906 cm^{-1}). For η_2-trans, this shift is stronger (from 1129 to 931 cm^{-1}).

For the bending modes, the $\delta(C_1H_1)$, $\delta(C_2H_2)$, and scissor $\delta(CH_3H_4)$ normal modes are weakly modified by the adsorption process so they cannot help to distinguish the sites. However, since the rocking mode $\rho(CH_3H_4)$ is strongly shifted to the high frequencies for η_2-trans (1117 cm^{-1}) and to the low frequencies for η_4-trans (914 cm^{-1}), it could be a good indicator for recognizing these adsorption forms. In contrast, the $\delta(C{-}C{=}O)$ and $\delta(C{=}C{-}C)$ bending vibrations are not characteristic of any adsorption structure.

For the torsion vibrations, the in-phase $\gamma^{ip}(CH)$ and out-of-phase $\gamma^{oop}(CH)$ modes are shifted toward the low frequencies for η_4-trans (746 and 849 cm^{-1} respectively). So they can help to recognize this site. The wagging $\omega(CH_3H_4)$ and twisting $\tau(CH_3H_4)$ modes are globally moved toward the high frequencies for all of the competitive sites. The soft twisting $\tau(C{-}C)$ mode in the 200 cm^{-1} region for the η_2 and η_3 families is useless to characterize the sites since it is not correctly treated in our method.

IV. Discussion

The comparison between the experimental HREELS and the theoretical EELS spectra requires a simulation of the EELS intensities and a thorough analysis of the stability of the adsorption sites. For a given coverage, the stable sites can be extrapolated from the adsorption energy diagram presented in Figure 2. For the low coverage region (below 0.15 ML), both η_3-cis and η_4-trans adsorption modes are competitive. As the coverage slightly increases (between 0.15 and 0.2 ML), the η_2-cis form becomes favorable. In the high coverage regime

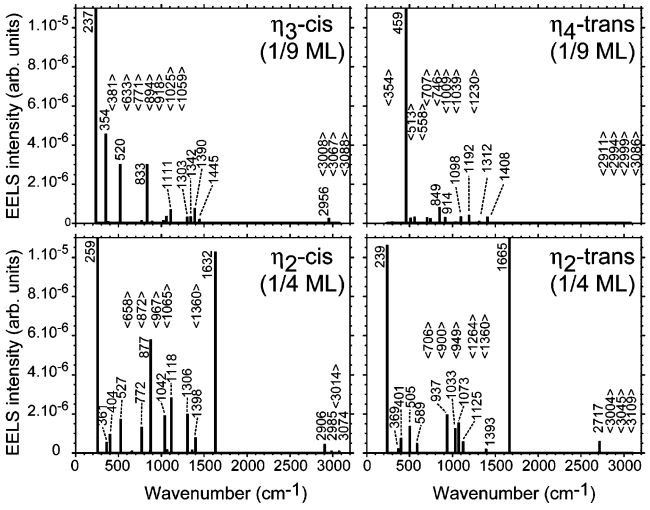

Figure 6. Simulated EELS spectra for the competitive η_3-cis, η_4-trans sites at low coverage 1/9 ML and η_2-cis and η_2-trans sites at higher coverage 1/4 ML. Some of the weakly intense and non active vibrations have been indicated in ⟨ ⟩.

(between 0.20 and 0.25 ML), the η_2 family is clearly the most stable one. So the DFT calculations suggest a progressive change of the adsorption modes upon coverage increase in favor of η_2-cis and η_2-trans.

The simulated spectra are given in Figure 6 for the four most stable adsorption modes, i.e., the η_3-cis and η_4-trans sites at 1/9 ML and the η_2-cis and η_2-trans sites at 1/4 ML. A direct comparison is proposed in Figure 7 between the experimental HREELS spectra obtained after an exposure of 1 and 2 L and the simulated ones for the η_3-cis mode and the η_2-cis one. For the purpose of simplicity, the calculated spectra of the two competitive sites (η_4-trans at 1/9 ML and η_2-trans at 1/4 ML) have not been reported in Figure 7. However, for the assignment of the experimental peaks, all of the specific active vibrations of these sites that help to complete the interpretation have been included in Figure 7. According to a previous infrared study of coadsorbed crotonaldehyde and CO on a Pt/TiO_2 catalyst,[32] the frequency shifts are small and are due to displacement of CO instead of electronic effects induced by coadsorption. As a consequence, the influence of the coadsorbed CO molecules is neglected in the following discussions.

If the bands resulting from the CO contamination are excluded (1860 and 2060 cm^{-1}), the spectrum for a low exposure of 1 ML shows very weak modes above 1000 cm^{-1}. This is in very good agreement with the flat η_3 and η_4 adsorption structures for which most vibrational modes are developed in a plane parallel to the surface and hence excluded from the surface dipole selection rule. Among the weak features, a wide band around 1370 cm^{-1} can be associated with several bands calculated for the η_3-cis structure at 1303 cm^{-1} ($\delta(C_1H_1)$), 1342 cm^{-1} ($\delta(C_2H_2)$), and 1390 cm^{-1} $\delta(CH_3H_4)$. The broad band at ~830 cm^{-1} can be related to the γ(CH) modes calculated at 833 cm^{-1} for η_3-cis and 849 cm^{-1} for η_4-trans. However, the most intense bands are located in the 350−500 cm^{-1} interval. They can be associated with the intense $\tau(C_1-C_2)$ mode at 459 cm^{-1} in the case of η_4-trans and with the δ(C═C−C) one at 354 cm^{-1} for η_3-cis. In addition, the ν(Pt−CO) vibration should also contribute to the observed band at 470 cm^{-1}.

Upon a larger exposure (2 L), new bands clearly develop on the spectrum. The most intense band at 1630 cm^{-1} can be associated with a change in binding site of acrolein from η_3-cis/η_4-trans to η_2-cis as a result of the higher coverage. This is fully consistent with the total energy calculations. Since the η_2-cis is only coordinated by the C═C bond and the C═O bond is tilted upward from the decoordination of the O atom, the ν(C═O) mode calculated at 1632 cm^{-1} contributes more effectively to the variation of the dipole moment z component (cf. Figure 8a) and hence becomes active. Several other modes also become more intense in the interval [1000−1500 cm^{-1}] and the apparition of η_2-cis molecules also explains, for the 2 L spectrum, the intensity at 1400 cm^{-1} from the $\delta(CH_3H_4)$ mode (calculated at 1398 cm^{-1}), at 1150 cm^{-1} from the ν(C═C) (calc. 1118 cm^{-1}), and at 1040 cm^{-1} from the $\rho(CH_3H_4)$ (calc. 1042 cm^{-1}). In the low-frequency region of the spectrum for 2 L exposure, the bands at 420 and 555 cm^{-1} can be associated to

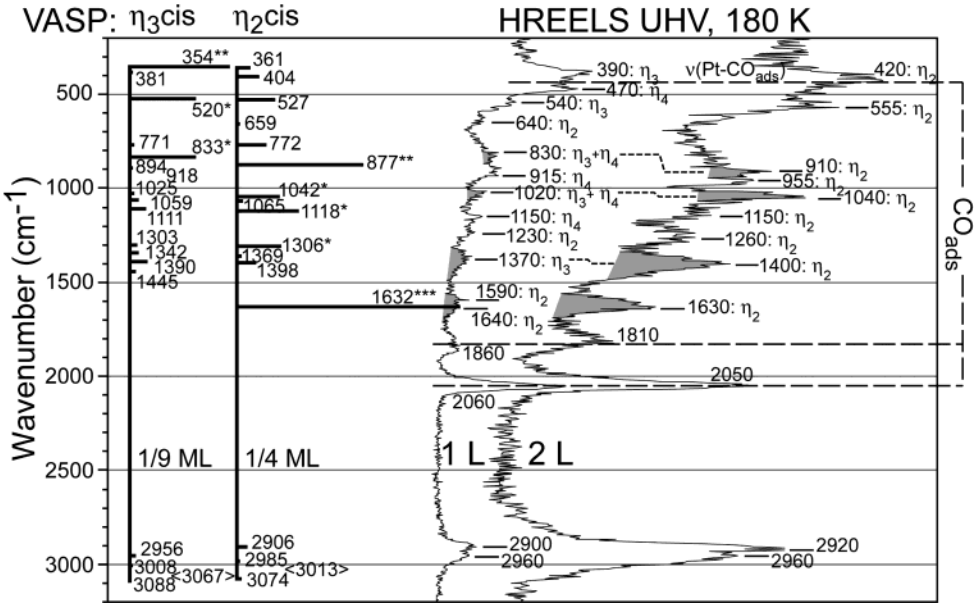

Figure 7. Comparison between the experimental 1 and 2 L HREELS spectra observed at 180 K (cf. Figure 4) and the simulated theoretical vibrational spectra for the competitive sites η_3-cis at low coverage 1/9 ML and η_2-cis at higher coverage 1/4 ML. On the experimental curves, the proposed assignments of the peaks are shown. Three vibrational bands which become significantly more intense at 2 L exposure are filled with grey. On the theoretical spectra, the activity of the modes is referenced with the number of asterisks: * accounts for weakly intense, ** for intense, *** for the most intense vibrations.

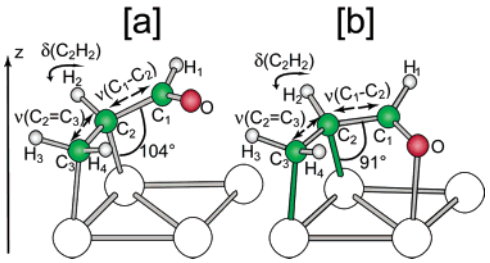

Figure 8. Schematic views of the vibrational coupling between the $\delta(C_2H_2)$ and $\nu(C{=}C)$ vibrations with the $\nu(C{-}C)$ stretch for the [a] η_2-cis and [b] η_3-cis sites. The vibrations are shown with black arrows and the variation of the $Pt{-}C_2{-}C_1$ bond angle (°) is reported.

molecule−surface stretching modes for the η_2-cis ($\nu_2(Pt{-}\eta)$ calculated at 404 cm^{-1} and $\nu_1(Pt{-}\eta)$ calculated at 527 cm^{-1}). Hence, the simultaneous explanation of many vibrational bands clearly validates the adsorption mode change at high coverage toward a predominant η_2-cis structure.

For the C−H high-frequency bands (cf. Table 4), the softest $\nu(C_1H_1)$ mode, which was expected to be the only C−H mode characteristic of an η_2 adsorption, is weakly active. This result agrees with the band measured in the 2906−2920 cm^{-1} region. In contrast, the measured band at 2960 cm^{-1} for the 1 L spectrum can be correlated with the weak intensity calculated at 2956 for η_3-cis.

If one observes with scrutiny the spectrum obtained after an exposure of 1 L, a very weak band can be seen at 1590−1640 cm^{-1}. This cannot be associated with a tiny activity of the $\nu(C{=}O)$ band for the flat modes predicted for such an exposure since the calculated frequencies are more shifted to the red in these modes where the π^*CO orbital directly interacts with the surface (1445 cm^{-1} for η_3-cis and 1192 cm^{-1} for η_4-trans). It must be related with a small fraction of η_2 adsorption already for the exposure of 1 L.

The main influence of the molecule coordination change from the flat η_3 and η_4 adsorption structures to the η_2 cis mode is hence an important increase of the intensity of several modes: $\nu(C{=}O)$, $\nu(C{=}C)$, $\nu(C{-}C)$, $\delta(C_2H_2)$, $\delta(CH_3H_4)$, and $\rho(CH_3H_4)$. The increased intensity for $\nu(C{-}C)$ at 877 cm^{-1} can be directly explained in a similar way as for the $\nu(C{=}O)$ mode. The Pt−O bond cleavage implies an opening of the bond angle $Pt{-}C_1{-}C_2$ from 91° to 104° resulting in a larger dynamic dipole for $\nu(C{-}C)$ along the *z* axis (cf. Figure 8a). The situation is more complex for $\nu(C{=}C)$ (1118 cm^{-1}) and $\delta(C_2H_2)$ (1306 cm^{-1}) since the C=C bond remains completely flat on the surface. This strengthening of the intensity can be explained by the vibrational coupling of $\nu(C{=}C)$ and $\delta(C_2H_2)$ with $\nu(C{-}C)$. An elongation along these modes is hence associated with a stretch of the C−C bond and a variation of the dipole moment *z* component, which explains their activity. In contrast, for η_3-cis (cf. Figure 8b), these couplings do not enhance the activity since all of the atoms involved in the coupled mode vibrate parallel to the surface ($\nu(C{-}C)$ itself is not active in this case).

V. Conclusion

New theoretical and experimental insights of the acrolein adsorption on Pt (111) are presented in this work. HREELS measurements extended to the high and low-frequency ranges have been reported at 180 K varying the exposure from 1 to 10 L. Total energy results show that the η_3-cis and η_4-trans sites are favored at low coverage (1/12→1/9 ML), whereas η_2-cis and η_2-trans structures become favorable near saturation (1/4 ML). The interpretation of the experimental spectra has been inferred from a combination of total energy calculations with EELS spectra simulations. The intensity change of the characteristic vibrational modes for η_3-cis and η_4-trans and η_2-cis and η_2-trans forms has allowed us to assign the 1 and 2 L low exposure HREELS spectra to a low coverage mixed phase (mainly η_3-cis and η_4-trans) and a high coverage mixed phase (mainly η_2-cis and η_2-trans), respectively. The most intense bands measured, for 2 L, at 1630, 1400, and 1040 cm^{-1} have been correlated with those calculated for $\nu(C{=}O)$ (1632 cm^{-1}), $\delta(C_2H_2)$ (1306 cm^{-1}), and $\nu(C{=}C)$ (1118 cm^{-1}) for the η_2-cis site (1/4 ML). The strengthening of these intensities has been elucidated by the vibrational coupling analysis of the $\delta(C_2H_2)$ and $\nu(C{=}C)$ modes vibrating parallel to the surface, with the nonparallel $\nu(C{-}C)$ mode.

The combined approach clearly shows that a strongly bound acrolein species is present on the surface at a temperature above 145 K. Below that temperature, a species more weakly bonded desorbs molecularly in the gas phase.[11] The structure of the strongly bonded species is coverage dependent, with a flat coordination by both the C=C and the C=O bond at low coverage and an adsorption only by the C=C bond at higher coverage. This contrast with previous conclusion from RAIRS[11] of an interaction mainly via the carbonyl group and has certainly important implications for the surface reactivity of the molecule.

The combination of density-functional theory predictions and vibrational spectroscopy measurements that has been used specifically for the case of acrolein on Pt(111) is of more general interest in heterogeneous catalysis. In fact, the vibrational characterization of these molecules based on combined experimental and theoretical approaches looks promising particularly for elucidation of reaction intermediates.

Acknowledgment. The authors thank the Institut du Développement et des Ressources en Informatique Scientifique (IDRIS) at Orsay, France (project 609) and the Centre Informatique National de l'Enseignement Supérieur (CINES) at Montpellier, France for CPU time and assistance. They also thank the GdR-Dynamique Moléculaire Quantique Appliquée à la Catalyse, a joint project of CNRS, Technische Universität Wien, and Institut Français du Pétrole. This project was possible due to the European Associated Laboratory between Leverhulme Centre for Innovative Catalysis and Institut de Recherches sur la Catalyse. The authors thank also CNRS-DFG bilateral project for financial support.

References and Notes

(1) Hoffmann, F. M. *Surf. Sci. Rep.* **1983**, *3*, 107−192.
(2) Ibach, H.; Mills, D. L. *Electron Energy Loss Spectroscopy and Surface Vibrations*; Academic Press: New York, 1982.
(3) Urban, M. W. *Vibrational Spectroscopy of Molecules and Macromolecules on Surfaces*; John Wiley & Sons: New York, 1993.
(4) Beccat, P.; Bertolini, J. C.; Gauthier, Y.; Massardier, J.; Ruiz, P. *J. Catal.* **1990**, *126*, 451−456.
(5) Gallezot, P.; Richard, D. *Catal. Rev.-Sci. Eng.* **1998**, *40*, 81−126.
(6) Marinelli, T. B. L. W.; Nabuurs, S.; Ponec, V. *J. Catal.* **1995**, *151*, 431−438.
(7) de Jesus, J. C.; Zaera, F. *J. Mol. Catal. A: Chem.* **1999**, *138*, 237−240.
(8) Claus, P. *Top. Catal.* **1998**, *5*, 51−62.
(9) Bournel, F.; Laffon, C.; Parent, P.; Tourillon, G. *Surf. Sci.* **1996**, *359*, 10−16.
(10) Bournel, F.; Laffon, C.; Parent, P.; Tourillon, G. *Surf. Sci.* **1996**, *350*, 60−78.
(11) de Jesus, J. C.; Zaera, F. *Surf. Sci.* **1999**, *430*, 99−115.
(12) Akita, M.; Osaka, N.; Itoh, K. *Surf. Sci.* **1998**, *405*, 172−181.
(13) Fujii, S.; Misono, Y.; Itoh, K. *Surf. Sci.* **1992**, *277*, 220−228.
(14) Fujii, S.; Osaka, N.; Akita, M.; Itoh, K. *J. Phys. Chem.* **1995**, *99*, 9, 6994−7001.
(15) Brown, N. F.; Barteau, M. A. *J. Am. Chem. Soc.* **1992**, *114*, 4258−4265.

(16) Yoshitake, H.; Iwasawa, Y. *J. Chem. Soc., Faraday Trans.* **1992**, *88*, 503−510.
(17) Delbecq, F.; Sautet, P. *J. Catal.* **2002**, *211*, 398−406.
(18) Kresse, G.; Hafner, J. *Phys. Rev. B* **1993**, *47*, 558−561.
(19) Kresse, G.; Hafner, J. *Phys. Rev. B* **1993**, *48*, 13115−13118.
(20) Kresse, G.; Furthmüller, J. *Phys. Rev. B* **1996**, *54*, 11169−11186.
(21) Perdew, J. P.; Wang, Y. *Phys. Rev. B* **1992**, *45*, 13244−13249.
(22) Vanderbilt, D. *Phys. Rev. B* **1990**, *41*, 7892−7895.
(23) Blom, C. E.; Müller, R. P.; Günthard, H. H. *Chem. Phys. Lett.* **1980**, *73*, 483−486.
(24) Blom, C. E.; Grassi, G.; Bauder, A. *J. Am. Chem. Soc.* **1984**, *106*, 7427−7431.
(25) Kuchitsu, K.; Fukuyama, T.; Morino, Y. *J. Mol. Struct.* **1967**−**1968**, *1*, 463−479.
(26) Kuchitsu, K.; Fukuyama, T.; Morino, Y. *J. Mol. Struct.* **1969**, *4*, 41−50.
(27) Pulay, P.; Fogarasi, G.; Pongor, G.; Boggs, J. E.; Vargha, A. *J. Am. Chem. Soc.* **1983**, *105*, 7037−7047.
(28) Hamada, Y.; Nishimura, Y.; Tsuboi, M. *Chem. Phys.* **1985**, *100*, 365−375.
(29) Loncharich, R. J.; Schwarz, T. R.; Houk, K. N. *J. Am. Chem. Soc.* **1987**, *109*, 14−23.
(30) Oelichmann, H.-J.; Bougeard, D.; Schrader, B. *J. Mol. Struct.* **1981**, *77*, 149−163.
(31) Thakur, S.; Gupta, V. P.; Ram, B. *Spectrochim. Acta Part A* **1997**, *53*, 749−759.
(32) Coloma, F.; Coronado, J. M.; Rochester, C. H.; Anderson, J. A. *Catal. Lett.* **1998**, *51*, 155−162.
(33) Alves, A. C. P.; Christoffersen, J.; Hollas, J. M. *Mol. Phys.* **1971**, *20*, 625−644.
(34) Osborne, G. A.; Ramsay, D. A. *Can. J. Phys.* **1973**, *51*, 1170−1175.